Supporting information

Dihydrophenazine Linked Porous Organic Polymers for High Capacitance and Energy Density Pseudocapacitive Electrodes and Devices

Huanhuan Zhang[a], Xiaohui Tang[a], Cheng Gu*[a, b]

[a]State Key Laboratory of Luminescent Materials and Devices, Institute of Polymer Optoelectronic Materials and Devices, South China University of Technology, No. 381 Wushan Road, Tianhe Distinct, Guangzhou, 510640, P. R. China.

[b]Guangdong Provincial Key Laboratory of Luminescence from Molecular Aggregates, South China University of Technology, No. 381 Wushan Road, Tianhe Distinct, Guangzhou, 510640, P. R. China.

Email: gucheng@scut.edu.cn

1. Experimental section

1.1 General: materials and instruments

All the chemical reactants for syntheis were purchased from J&K and used as received. Electrolyte (1 M Et_4NBF_4 in superdry propylene carbonate, H_2O content less than 20 ppm) for the electrochemical characterization and device assembly was perchased from Capchem Inc., Shenzhen. Super P and PVDF were purchased from MTI Co., Shenzhen. Active carbon (YEC-8, BET 2000~2500 $m^2\ g^{-1}$) was purchased from Yihuan Carbon Co., Fuzhou. Glass microfiber filter (Whatman GF-D, thickness 675 μm, diameter 16 mm) is used as separator. The components of the CR2032 button battery (including positive and negative cases, gasket and shrapnel) are made of stainless steel, model 316, and ultrasonically cleaned with water and ethanol before use.

Scanning electron microscope (SEM) images were recorded by a Hitachi Regulus 8100. The Fourier transform infrared spectroscopy (FTIR) was recorded by IFS 66V/S Fourier transform infrared spectrophotometer. X-ray photoelectron spectroscope (XPS) was characterized on Kratos Axis Ulra DLD. X-ray diffraction (XRD) spectrum was recorded on Rigaku SmartLab SE. Ultraviolet and visible (UV-vis) spectra were recorded on Shimadzu UV-3600 spectrometer. Elemental analysis was performed on Elementar Vario EL elemental analyzer. Thermal Gravimetric Analysis (TGA) was performed on Rigaku Thermo plus EVO2 under N2, by heating to 500 °C at a rate of 5 °C min^{-1}. High-resolution transmission electron microscopy (HR-TEM) images were obtained on a TEM JEOL 2100F with an acceleration voltage of 300 kV. The electronic conductivity was recorded with a Keithley 2400 source meter.

1.2 Synthesis

5,10-dihydrophenazine: Phenazine (3 g, 16.6 mmol) was added into 40 mL of boiling ethanol in a 500 mL two-neck flask with stirring bar. A suspension of sodium dithionite (26 g) in deionized water (200 mL) was added dropwise into the phenazine solution. Afterwards, the mixture was vigorously stirred for 3 h. The resulting grey-white precipitate was filtered and washed for several times with deionized water and ethanol. The collected solid was dried under reduced pressure to afford product (2.91 g, yield = 96%). This material was directly used in the next step without further purification.

4,4'-(phenazine-5,10-diyl) dibenzonitrile (DHPAZ-2CN): A mixture of 5, 10-dihydrophenazine (1092 mg, 6 mmol), 4-bromobenzonitrile (2730 mg, 15 mmol), potassium carbonate (4968 mg, 36 mmol), tri-tert-butylphosphine (244.8 mg, 1.21 mmol), palladium (II) acetate (100 mg) and toluene (30 mL) was refluxed at 110 °C for 24 h under nitrogen. After the system was cooled down, 30 mL dichloromethane and 20 mL deionized

water were added to the resulting mixture. The organic phase was extracted with dichloromethane for three times. The combined organic layers were dried with $MgSO_4$ and concentrated under reduced pressure. The obtained solid was purified by chromatography with a mixture of dichloromethane/petroleum ether (v/v =1/1) as the eluent to afford DHPAZ-2CN as orange solid (1.5 g, yield = 67%). The product was further purified by sublimation under reduced pressure. ^{1}H NMR (500 MHz, DMSO-d_6): δ (ppm) = 5.91 (dd, *J* = 5.9, 3.4 Hz, 4H), 6.54 (dd, *J* = 5.9, 3.4 Hz, 4H), 7.62 (d, *J* = 8.5 Hz, 4H), 8.10 (d, *J* = 8.5 Hz, 4H). ^{13}C NMR (126 MHz, DMSO-d_6): δ (ppm) = 144.29, 134.89, 129.62, 121.65, 117.87, 114.10, 109.65; APCI MS: calcd. for $[M]^+$, *m/z* = 384.14; found *m/z* = 384.

GT-POP-1: DHPAZ-2CN (100 mg, 0.26 mmol) was placed in a 10 mL shrek tube. Triflic acid (2 mL) was added dropwise to shrek tube at -10 °C under N_2 in 5 min. The resulting solution was stirred for 1.5 h at -10 °C. The solution was further stirred for another 12 h at 60 °C. After cooling down to room temperature, the reaction was quenched by 2 M NaOH aqueous solution. Then the resulting precipitate was filtered and washed with 2 M NaOH and deionized water. The collected solid was soxhleted with dichloromethane (48 h), acetonitrile (24 h) and methanol (24 h), respectively. The powder was dried in vacuum oven to afford GT-POP-1 as a brownish-red powder (54 mg, yield = 54%).

CTF-400: $ZnCl_2$ was used as catalysis and solvent at the same time. DHPAZ-2CN (384 mg, 1 mmol) and anhydrous $ZnCl_2$ (681 mg, 5 mmol) were mixed in glovebox and transferred into a glass ampule. The ampule was evacuated by vacuum pump, sealed and heated at the rate of 5 °C min^{-1} to 400 °C and maintained at this temperature for 40 h. Then the ampule was cooled to room temperature. The product was washed thoroughly with 5% HCl solution, deionized water and tetrahydrofuran, and then dried under vacuum at 120 °C for 12 h to get the dark brown powder.

1.3 Electrode fabrication

Active materials, Super P and poly(vinylidene fluoride) with a weight ratio of 5:4:1 were immersed in small amount of N-Methyl pyrrolidone (NMP) and thoroughly mixed by a planetary mill at a speed of 400 rpm for 3 min. Then the mixture was solution-cast onto aluminum foil with a thickness of 100 μm using doctor blade method. To remove NMP and trace water, electrodes were transferred into vacuum oven and heated at 80 °C for 24 h before being cut into circles with a diameter of 12 mm.

1.4 *Electrochemical characterizations of single electrode*

Cyclic voltammetry and AC impedance tests were performed in an inert N_2 atmosphere glove-box using an Autolab electrochemical workstation, PGSTAT302N. The configuration of electrolyte cell is one-room, three-electrode with active materials as working electrode, spiro platinum wire (8 cm in length, 5 mm in diameter) as counter electrode, Ag/Ag^+ (0.01 M $AgNO_3$) as reference electrode. AC impedance tests were carried out at open circuit potential, from 1 MHz to 0.1 Hz with excitation amplitude of 10 mV. The equivalent circuits were fitted by the Nova software attached with the Autolab workstation. Galvanic charge/discharge tests were conducted on a CT2001A purchased from LAND Electronic Corporation, Wuhan, China.

1.5 *Supercapacitor device assembly*

The supercapacitor devices were assembled by placing the separator (Whatman glass microfiber filter, GF-D, thickness 675 μm, 16 mm in diameter) between negative (active carbon) and positive (GT-POP-1) electrodes. Then immersed the sandwich devices in about 0.5 ml electrolyte. The devices were sealed in CR2032 button cells and placed in the glove box overnight to allow the electrolyte evenly penetrate into electrodes.

1.6 *Computational method*

The GT-POP-1 membrane was prepared by drop casting its solution in N,N-dimethylformamide onto nonconductive glass substrate followed by thermal evaporation of the solvent. Silver electrodes were prepared on the surface of membranes by vacuum deposition through contact shadow mask. The electronic conductivity of GT-POP-1 was calculated by the following equation:

$$\sigma = \frac{d}{R\,l\,t} \tag{1}$$

where σ is the conductivity (S cm^{-1}), d is the distance of the two silver electrodes (2 mm), l is the length of the electrodes (1 cm), and t and R are the thickness (20 μm) and resistance (Ω, calculated from the I-V curve) of GT-POP-1 membrane, respectively.

The quantitative analysis of element contents in XPS is performed according to the following equation.

$$\frac{N_x}{N_y} = \frac{A_x}{A_y} \times \frac{S_x}{S_y} \tag{2}$$

where $N_x\,(N_y)$, $A_x\,(A_y)$ and $S_x\,(S_y)$ are the molar content, integration area and sensitiviy factor of element x (y), respectively.

The areal capacitance of electrode and cell can be obtained from discharge profile in CCCD test based on the equation below:

$$C = \frac{It}{VA} \tag{3}$$

where *I* is the discharge current density, *t* is the time during the discharge process and V is the potential, *A* is the area of electrode (or mass of the active materials). The area energy density and power density of supercapacitor devices can be calculated by using the following equations:

$$E = \frac{CV^2}{2 \times A \times 3600} \tag{4}$$

$$P = \frac{E}{t} \times 3600 \tag{5}$$

where *V* is the voltage, A is the sum of the area (or mass) of the two electrodes and *t* is the discharge time.

2. Characterizations

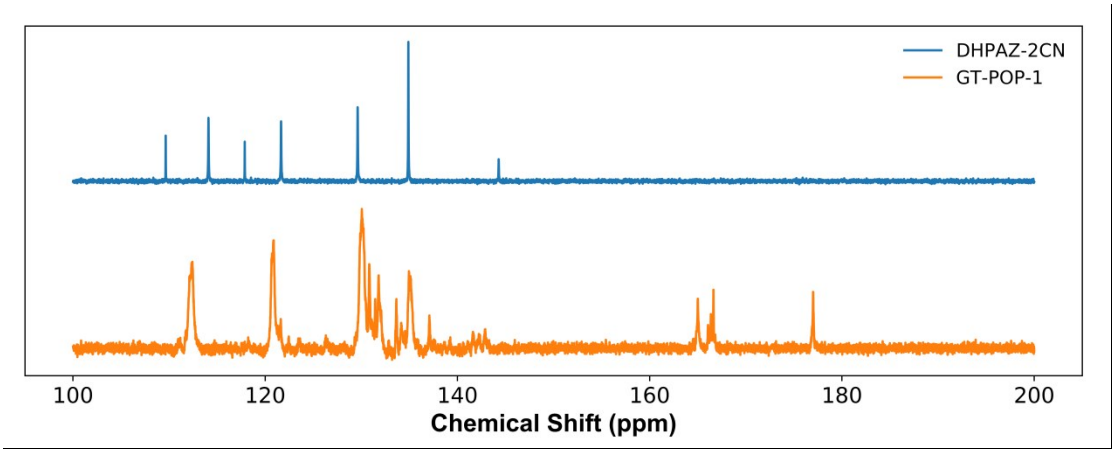

Fig. S1. ^{13}C NMR spectra of GT-POP-1 and its monomer DHPAZ-2CN tested in DMSO-d_6.

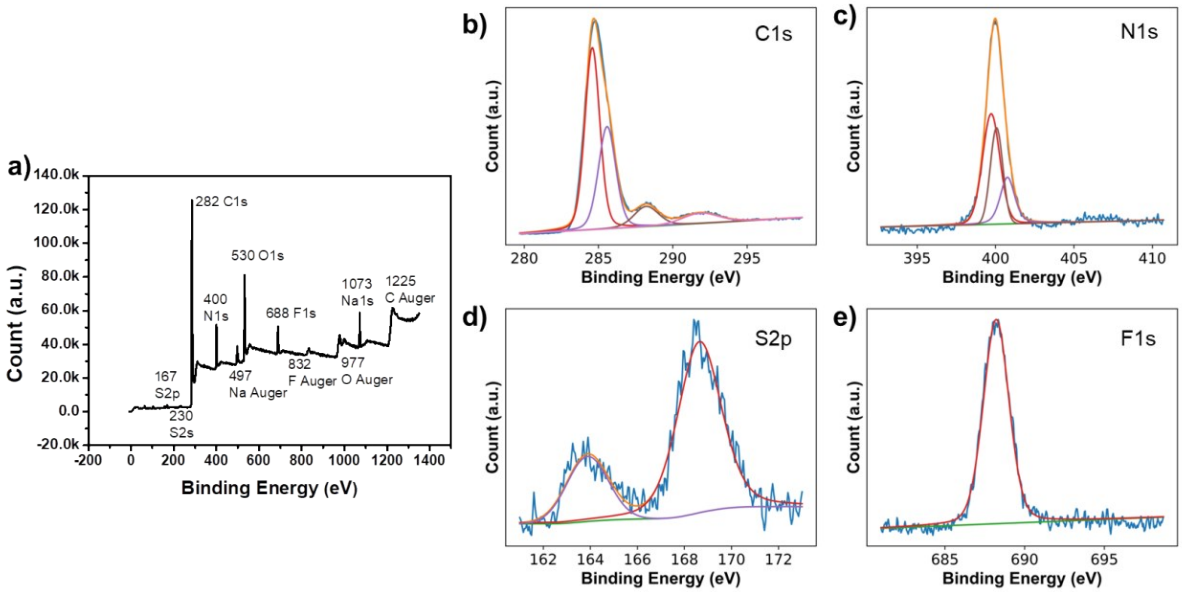

Fig. S2. XPS of GT-POP-1: a) full scan; b) C1s; c) N1s d) S2p and e) F1s.

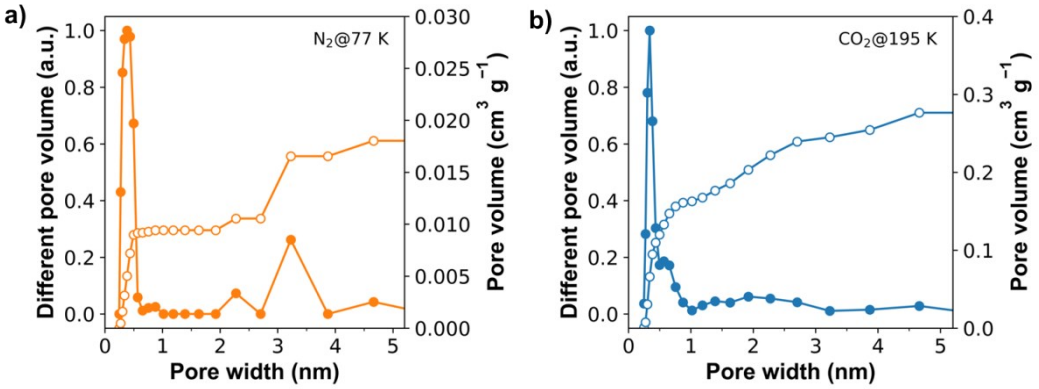

Fig. S3. Pore size distributions of GT-POP-1 measured at N_2 77 K and CO_2 195 K.

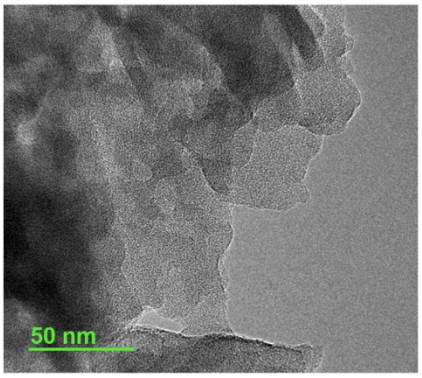

Fig. S4. HR-TEM image of GT-POP-1.

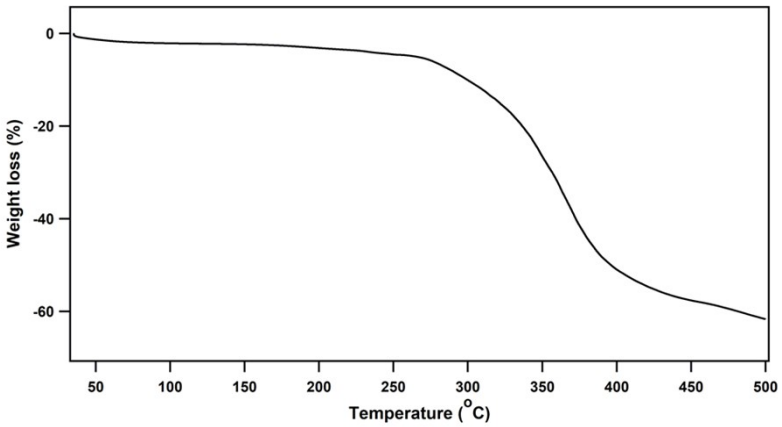

Fig. S5. TGA curve of GT-POP-1 measured under N2, by heating up to 500 °C at a rate of 5 °C min^{-1}.

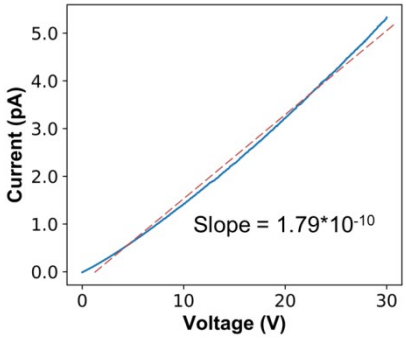

Fig. S6. I-V curve of GT-POP-1. The calculated electronic conductivity is to be 1.8 × 10^{-8} S cm^{-1}.

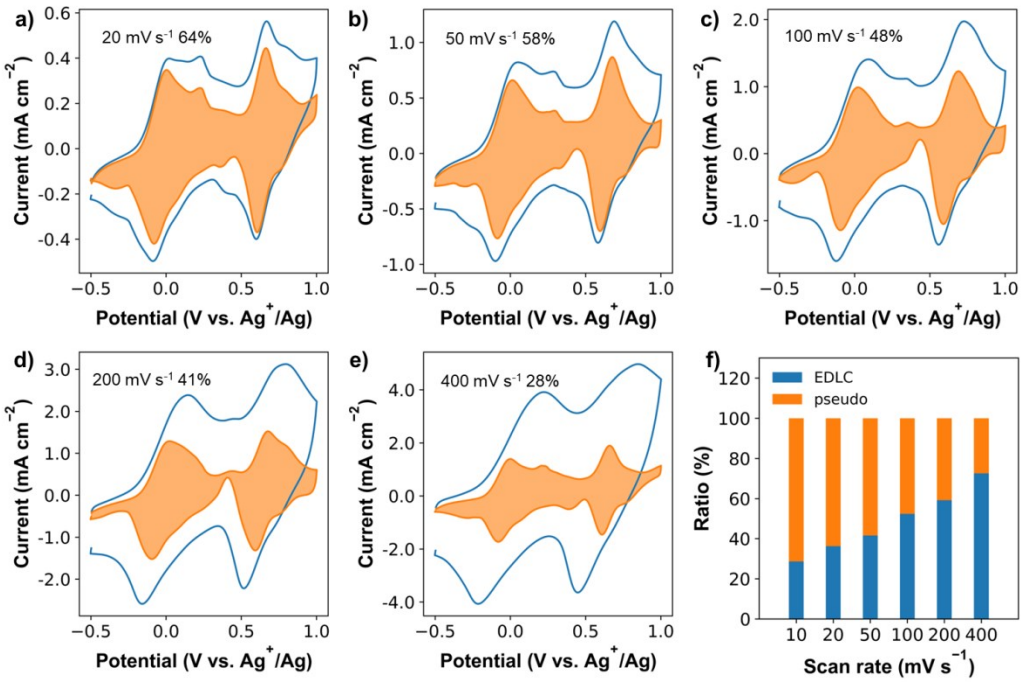

Fig. S7. Kinetic analysis at different scan rate of a-e) 20, 50, 100, 200 and 400 mV s^{-1}. The total current (solid blue line) is obtained experimentally. The shaded regions show the contribution of pseudocapacitance at different scan rates as a function of potential; f) EDLC and pseudocapacitance contribution ratio bar at different scan rates.

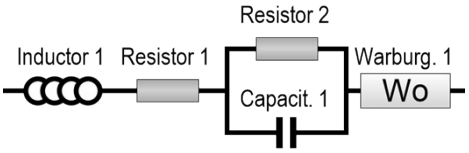

Fig. S8. Equivalent circuit of impedance fitting.

Table S1. Elements values fitted by the equivalent circuit in Fig. S8.

Name	Value	Error	
Inductance 1	1.11E-06	1.04E-08	0.93%
Resistance 1	3.314232262	0.019395811	0.59%
Resistance 2	6.877610254	0.064823818	0.94%
Capacitance 1	1.86E-06	2.52E-08	1.35%
Wo. Zw 1	6.664311161	0.334378669	5.02%
Wo. tau 1	0.003586108	0.000194783	5.43%
Wo. alpha 1	0.483932789	0.00087334	0.18%

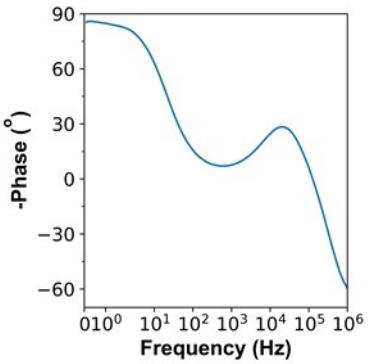

Fig. S9. Bode plot of the GT-POP-1//AC asymmetric supercapacitors.

Table S2. Comparison of energy density, power density and retention for selected supercapacitor devices.

Device	**Electrolyte**	**Voltage**	**Ed**	**Pd**	**Retention, cycles**	**Ref.**
RuO_2//Hex-Aza-COF-3	1 M H_2SO_4	1.7 V	23.3 W h kg^{-1}	661.2 W kg^{-1}	89%, 7500	1
TpOMe-DAQ	2 M H_2SO_4/PVA	1 V	2.9 μWh cm^{-2}	61.8 μW cm^{-2}	65%, 50000	2
Dq1Da1TpCOF	1 M H_2SO_4	1 V	0.43 μWh cm^{-2}	980 μW cm^{-2}	90%, 2500	3
CAP-2//AC	2 M KCl	1.6V	23 Wh kg^{-1}	-	80%, 10000	4
MnO_2//rGO	1 M Na_2SO_4	1.5 V	11.5 μWh cm^{-2}	3.8 mW cm^{-2}	93%, 3600	5
CoO_x// Fe_3O_4	6 M KOH	1.7 V	45.3 Wh kg^{-1}	1010 W kg^{-1}	91.8%, 5000	6
P3MT/HACNT //HACNT	1 M Et_4NBF_4	3.5 V	1.08 mWh cm^{-2}	1.75 W cm^{-2}	92%, 5000	7
GT-POP-1//AC	**1 M Et_4NBF_4**	**2.8 V**	**23.3 Wh kg^{-1} 7.2 μWh cm^{-2}**	**9642 W kg^{-1} 2986 μW cm^{-2}**	**84%, 2000**	**This work**

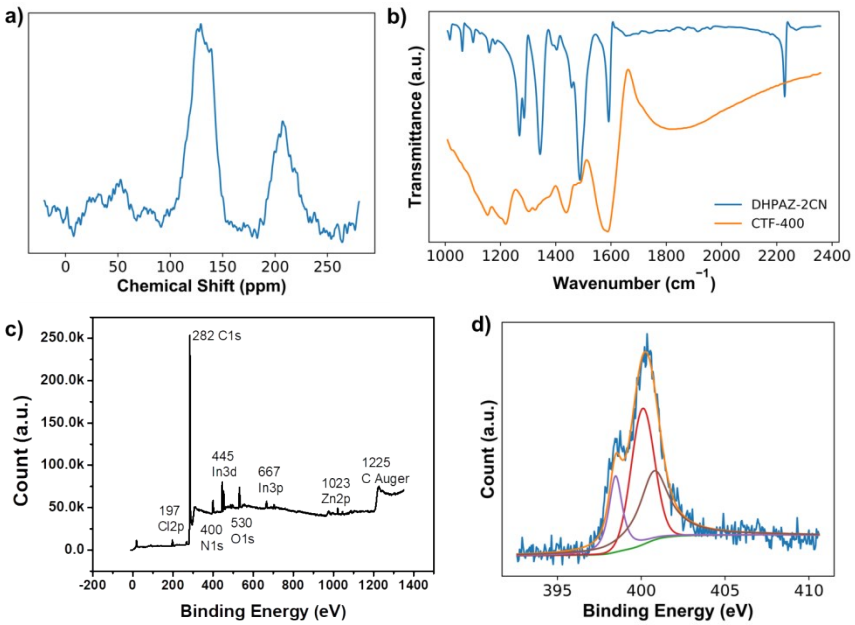

Fig. S10. Structure characterizations of CTF-400: a) Solid ^{13}C NMR; b) FT-IR spectrum; XPS analysis of c) full scan and d) deconvoluted N1s.

The ^{13}C NMR revealed strong bands at 180~240 ppm which might be attributed to the C=O formed under high temperature. In consistency with this, the broad band at 1700~2200 cm^{-1} in FT-IR spectrum also implied the formation of N=C=O. XPS full scan presented that there was residue $ZnCl_2$ in the product. To clarify, the In3d and In3p signals might be caused by the ITO substrate which we used to support the CTF-400 powder. The deconvoluted peaks in N1s spectrum at 398.5, 400.1 and 400.8 eV might be attributed to pyridinic nitrogen, pyrrolic nitrogen, and tertiary quaternary nitrogen, respectively, suggesting that some rearrangement reactions or even decomposition reactions may occur under the synthesis condition[8].

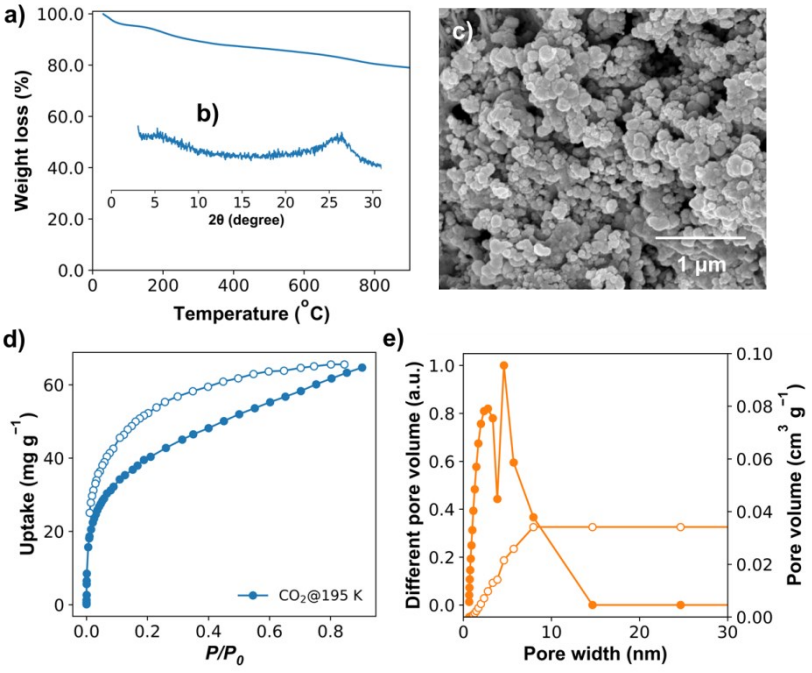

Fig. S11. Property measurements of CTF-400: a) TG analysis; b) PXRD pattern; c) SEM image; d) gas

adsorption/desorption isotherm curves at CO_2 195 K and corresponding e) pore size distribution analysis.

The TG analysis showed that CTF-400 keeps stable above 800 °C (**Fig. S11a**). The PXRD pattern indicated the amorphous nature (**Fig. S11b**). Scanning electron microscopy (SEM) images also verified this property (**Fig. S11c**). We measured the N_2 uptake of CTF-400 at 77 K for 3 days and no absorption was observed. The adsorption/desorption isothermal curves in CO_2 at 195 K is presented in **Fig. S11d.** The calculated BET surface area was only 12 m^2 g^{-1} and the pore size distribution analysis revealed the mesoporous structure of CTF-400 (**Fig. S11e**).

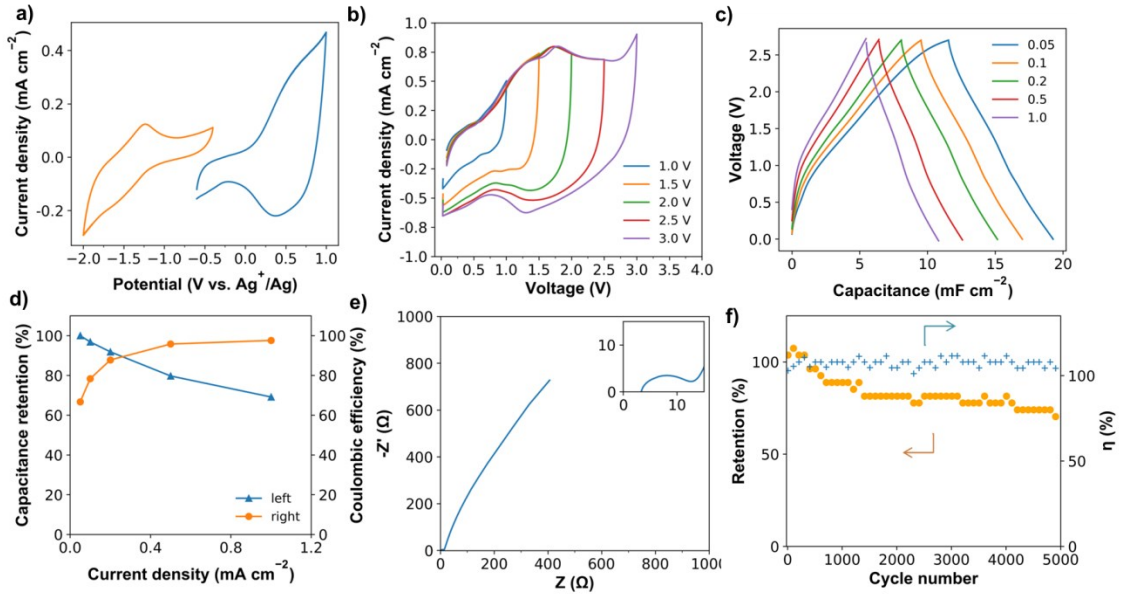

Fig. S12. a) Electrochemical characterization of CTF-400 in three-electrode-configuration encompassing cathodic and anodic scan; supercapacitive performance of CTF-400//AC asymmetric device: b) CV curves at different cutting off voltages of 1.0, 1.5, 2.0, 2.5V and 3.0 V; c) galvanostatic charge/discharge at different current densities of 0.05, 0.1, 0.2, 0.5, 1.0 mA cm^{-2}; d) capacitance retention and coulombic efficiency calculated from the discharge curves; e) Nyquist plots (inset is the enlarged part at high frequency region); f) repeated charge/discharge stability (capacitance retention and coulombic efficiency η).

3. References

1. S. Kandambeth, J. Jia, H. Wu, V. S. Kale, P. T. Parvatkar, J. Czaban‐Jóźwiak, S. Zhou, X. Xu, Z. O. Ameur, E. Abou‐Hamad, A. H. Emwas, O. Shekhah, H. N. Alshareef and M. Eddaoudi, *Adv. Energy Mater.*, 2020, DOI: 10.1002/aenm.202001673.
2. A. Halder, M. Ghosh, M. A. Khayum, S. Bera, M. Addicoat, H. S. Sasmal, S. Karak, S. Kurungot and R. Banerjee, *J. Am. Chem. Soc.*, 2018, **140**, 10941-10945.
3. M. A. Khayum, V. Vijayakumar, S. Karak, S. Kandambeth, M. Bhadra, K. Suresh, N. Acharambath, S. Kurungot and R. Banerjee, *ACS Appl. Mater. Interfaces*, 2018, **10**, 28139-28146.
4. W. Liu, M. Ulaganathan, I. Abdelwahab, X. Luo, Z. Chen, S. J. Rong Tan, X. Wang, Y. Liu, D. Geng, Y. Bao, J. Chen and K. P. Loh, *ACS Nano*, 2018, **12**, 852-860.
5. A. Sumboja, C. Y. Foo, X. Wang and P. S. Lee, *Adv. Mater.*, 2013, **25**, 2809-2815.
6. J. Zhu, L. Huang, Y. Xiao, L. Shen, Q. Chen and W. Shi, *Nanoscale*, 2014, **6**, 6772-6781.
7. Y. Zhou, X. Wang, L. Acauan, E. Kalfon-Cohen, X. Ni, Y. Stein, K. K. Gleason and B. L. Wardle, *Adv. Mater.*, 2019, **31**, 1901916.
8. L. Hao, B. Luo, X. Li, M. Jin, Y. Fang, Z. Tang, Y. Jia, M. Liang, A. Thomas, J. Yang and L. Zhi, *Energy Environ.*

Sci., 2012, **5**, 9747-9751.